Journal of Coastal Research	11	4	1258–1271	Fort Lauderdale, Florida	Fall 1995

Wave Transformation Near Virginia Coast: the "Halloween" Northeaster

Jerome P.-Y. Maa† and David W.-C. Wang‡

†School of Marine Science
Virginia Institute of Marine Science
College of William and Mary
Gloucester Point, VA 23062, U.S.A.

‡Computer Sciences Corporation
Stennis Space Center MS 39529, U.S.A.

ABSTRACT

MAA, J.P.-Y. and WANG, D.W.-C., 1995. Wave transformation near Virginia coast: the "Halloween" Northeaster. *Journal of Coastal Research*, 11(4), 1258–1271. Fort Lauderdale (Florida). ISSN 0749-0208.

The "Halloween" Northeaster of October 29–31, 1991 generated severe seas; the maximum wave height and peak wave period reached 8 m and 20 s at an offshore wave station located at the continental shelf break about 100 km off the Virginia coast. Storm waves were also measured shoreward at a nearshore wave station located at the Chesapeake Bay Light Tower, which is about 25 km east of the Chesapeake Bay mouth. The wave spectra at these two stations were quite different. We split the measured offshore wave spectra into seven or eight frequency bands and calculated the representative wave heights, periods, and deepwater wave directions for each band. We then used this offshore wave information, the RCPWAVE wave model, a numerical scheme for calculating wave height attenuation caused by bottom friction, and the given bathymetry to evaluate the following four wave transformation processes: refraction, diffraction, shoaling, and bottom friction. We found that bottom friction is an important factor that affects wave transformation between the two stations. If the effects of bottom friction are excluded, the calculated wave spectra at the nearshore station would be much larger than the measurements. Using small constant wave friction factors ($f_w = 0.01$ for frequency ≤ 0.07 Hz, $f_w = 0.02$ for 0.07 Hz $<$ frequency $<$ 0.08 Hz, and $f_w = 0.03$ for frequency ≥ 0.08 Hz), we can reasonably reconstruct the wave spectra at the nearshore station. This small variation of f_w for a rather large frequency band (from 0.045 to 0.115 Hz) might imply that other processes are also responsible for the significant wave damping. The accuracy of deepwater incident wave angles and the directional spreading are critical to reconstruct wave spectra at the nearshore station. The Norfolk Canyon at the continental shelf break has a significant influence on the spectral transformation of these "Halloween" storm spectra because of the long-period wave components.

ADDITIONAL INDEX WORDS: *Storm waves, wave spectra, wave transformation processes, wave station, deepwater waves.*

INTRODUCTION

Northeasters, extratropical storms that occur off the northeast coast of the United States, are a major threat to marine navigation, offshore operations, beaches, and coastal structures. Although extratropical storms are generally less powerful than hurricanes with respect to wind strength, the longer duration of such storms over a longer fetch can generate waves that exceed those from hurricanes.

In late October 1991, the most powerful northeaster (actually a combination of a low pressure center and Hurricane Grace) in the last 50 years developed off the Atlantic coast of North American (DOLAN and DAVIS, 1992). The location of the low pressure centers of the two storms, identified by the solid circles at six hour intervals, are shown in Figure 1. Severe seas generated by the storm pounded the east coast from Nova Scotia to Florida for 72 hours. The maximum significant wave height at a wave station of the National Data Buoy Center (NDBC) in the North Atlantic Ocean reached 12 m (WANG and METTLACH, 1992). Detailed descriptions of the evolution of this storm can be found in DOLAN and DAVIS (1992) and PUSCH and AVILA (1992).

There are two wave stations off the Virginia coast: A moored buoy station, 44014, located near the continental shelf break in a water depth of 48 m (Longitude 74°50′01″, Latitude 36°34′59″); and a Coastal-Marine Automated Network (C-MAN) station, CHLV2, located on a small shoal approximately 25 km east of the Chesapeake Bay mouth in a water depth of 12 m (Longitude 75°42′48″, Latitude 36°54′18″). However, the water depth around the shoal is about 20 m. Although only station 44014 provides directional wave infor-

94015 received 10 February 1994; accepted in revision 15 June 1994.

mation, both recorded the complete history of this storm. The wave spectra at these two stations clearly show the passing through of huge swells generated far away from the north Atlantic Ocean. The quite different wave spectra measured from the two stations also mark a significant wave damping. The valuable wave data may be used to study wave transformation at the continental shelf because of the unique long-period waves.

Wave transformation includes many processes, *e.g.*, wave shoaling, refraction, diffraction, reflection, nonlinear interaction, bottom friction, percolation losses, wind energy input, wave irregularity, wave directional spreading, wave-wave interaction, white capping, wave breaking, and wave-current interaction. It is difficult to simulate all these processes using a single computer program. Although wave transformation is a combination of the above mentioned processes, not all processes are equally important for all cases. In general, the most important processes are wave refraction, diffraction, and shoaling. In the past two decades, numerical models that simulate the three major processes for wave transformation have been attempted extensively (BERKHOFF *et al.*, 1982; LIU and TSAY, 1985; LIU *et al.*, 1986; KIRBY, 1986a, 1986b, 1988; EBERSOLE *et al.*, 1986; PANCHANG *et al.*, 1988; SUH and DALRYMPLE, 1993). Spectral wave transformation models that tried to include all major processes, *e.g.*, the model given by CHEN and WANG (1983), IZUMIYA and HORIKAWA (1987), BRIGGS *et al.* (1989), CHIAIA *et al.* (1990), or ABREU *et al.* (1992), have also been developed to mimic the wave spectrum transformation. Ideally a spectral wave transformation model should have been used to study the causes of the drastic difference of wave spectra between station 44014 and CHLV2. These models, however, are fairly complicated and not available. Thus, we used the RCPWAVE model developed by the U.S. Army Corps of Engineers (EBERSOLE *et al.*, 1986) to study the wave refraction, diffraction, and shoaling.

We were also interested in the effect of wave energy loss caused by sandy bottom on the wave transformation because of the long wave travel distance, 87 km. The procedure presented by MAA and KIM (1992) to calculate wave energy loss caused by bottom friction was simplified and used in this study. Wave energy loss caused by percolation (REID and KAJIURA, 1957; summarized in DEAN and DALRYMPLE, 1992) was also examined. Because of the extraordinary long-period waves,

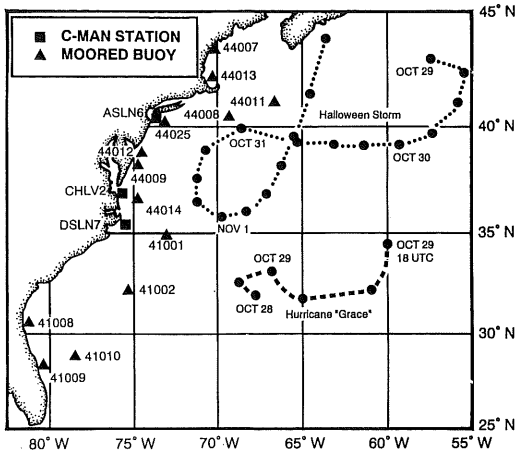

Figure 1. Locations of NDBC Wave Stations and central trajectories of the "Halloween" Northeaster and the Hurricane Grace.

the influence of wind energy input (mainly in the high frequency domain) on the wave transformation may be neglected.

Field data for wave transformation, especially for extreme events, are scarce. Thus, we would like to present the records and study the possible reasons that cause the significant differences in wave spectra between these two stations.

WAVE STATIONS AND MEASUREMENT DEVICES

The National Data Buoy Center has 16 stations located along the eastern coasts of the United States (WANG and METTLACH, 1992), both moored buoys and C-MAN stations. Figure 1 shows the locations of these stations.

The wave measurement system on the moored buoys employs an accelerometer to record buoy heave motion. A NDBC onboard Wave Data Analyzer computed the wave spectral information from the time series of buoy motion and transmitted the results to the Stennis Space Center in Mississippi for further analysis and quality assurance. Among these stations, station 44014 (sponsored by the U.S. Army, Coastal Engineering Research Center) also provided wave directional information by measuring the buoy's heave, pitch, and roll motions based on the approach proposed by LONGUET-HIGGINS *et al.* (1963).

Wave measurements at the C-MAN stations

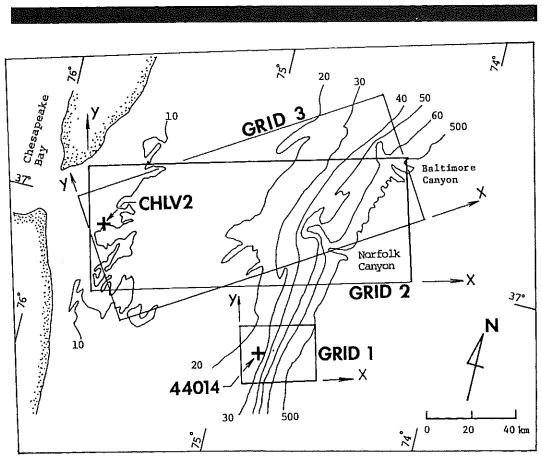

Figure 2. The study area (depth contours in fathom) and the grids for study wave transformation. Wave stations ares marked by '+'.

were carried out with the Infrared Laser Wave Height Sensor, which measured the surface displacement. The overall accuracy of all systems for significant wave height, wave period, and wave direction is 0.2 m (or 5%), 1.0 sec, and ±5°, respectively (MEINDL and HAMILTON, 1992). Details of the NDBC wave measurement system and data processing technique can be found in STEELE *et al.* (1990). For this storm, we will concentrate on stations 44014 and CHLV2. WANG and METTLACH (1992) reported the storm wave information for other stations.

The study site is shown in Figure 2. The upper left corner of the study area is the Chesapeake Bay mouth. Depth contours shown in Figure 2 are duplicated from chart. Digital bathymetric data for this area are available from the National Geophysical Data Center, NOAA, Dept. of Commerce. These data, however, are irregularly spaced. The density of data point is good for near shore area (within 40 km from the coast). Further offshore, the density decreases. To use these digital data for the RCPWAVE model, three evenly spaced bathymetric data matrices (with space 160 m in the x direction and 200 m in the y direction) were generated using the inverse distance method and Octant search method. The enclosed areas for these matrices are marked as Grid 1, 2, and 3 in Figure 2. For this reason, the original bathymetry has been smoothed slightly. Other than that, no other smoothing process has been made in this study. More details of the grid selection will be given later in this paper. The two stations are marked by the signs '+' in Figure 2.

WAVE RECORDS

Figure 3 shows the evolution of significant wave height, peak wave period, and local wind speed at the two stations. At station 44014, wave energy reached its maximum on October 31, 03 hr. All times used in this paper are Greenwich Mean Time (GMT). At station CHLV2, the maximum occurred 1 to 2 hr later because of the time required for the waves to travel across the continental shelf. In this study, we may reasonably assume that the spatial variation of deepwater waves off the continental shelf break is small.

For most of October 28, the significant wave height at station 44014 was about 3 m and gradually increased to 4.5 m by October 29. It remained at that level for the next 36 hours, then began to increase for the next 17 hours and reached its maximum (8.04 m) on October 31, 03 hr. Apparently the severe wave conditions were due to the arrival of long-period waves. After the peak, the significant wave height decreased slowly to 2 m in about 45 hours.

The significant wave height at station CHLV2 was about 1.5 m at the beginning of October 28. It increased from 1.5 m to 3.7 m during the last 12 hours of October 28 and remained at 3.7 m for an additional 8 hours. It then decreased slowly to 3 m by the middle of October 29 and stayed at that level until October 31 (despite the increase in wave height at station 44014 commencing on midday of October 30). The significant wave height increased quickly to 3.9 m in 3 hours and remained at that level for another 4 hours before a slow decrease. Notice that the significant wave heights at CHLV2 on the beginning of October 29 are similar to those at station 44014 (3.8 m versus 4.2 m) because of the prevailing local wind waves at that time (judged by the peak wave periods, 8 to 9 sec, and wind speed records at these two stations, see Figure 3C).

Figure 4 shows the comparison of peak storm wave spectra (Oct. 31, 03:00) between these two stations. Because of the time required for waves to cross the continental shelf and the different speeds for each wave component, we compared the spectrum at station 44014 (solid line) with the average of three consecutive wave spectra from station CHLV2 (dashed line). The vertical bars indicate the range of wave energy spectrum for the three consecutive hours. At station 44014, the

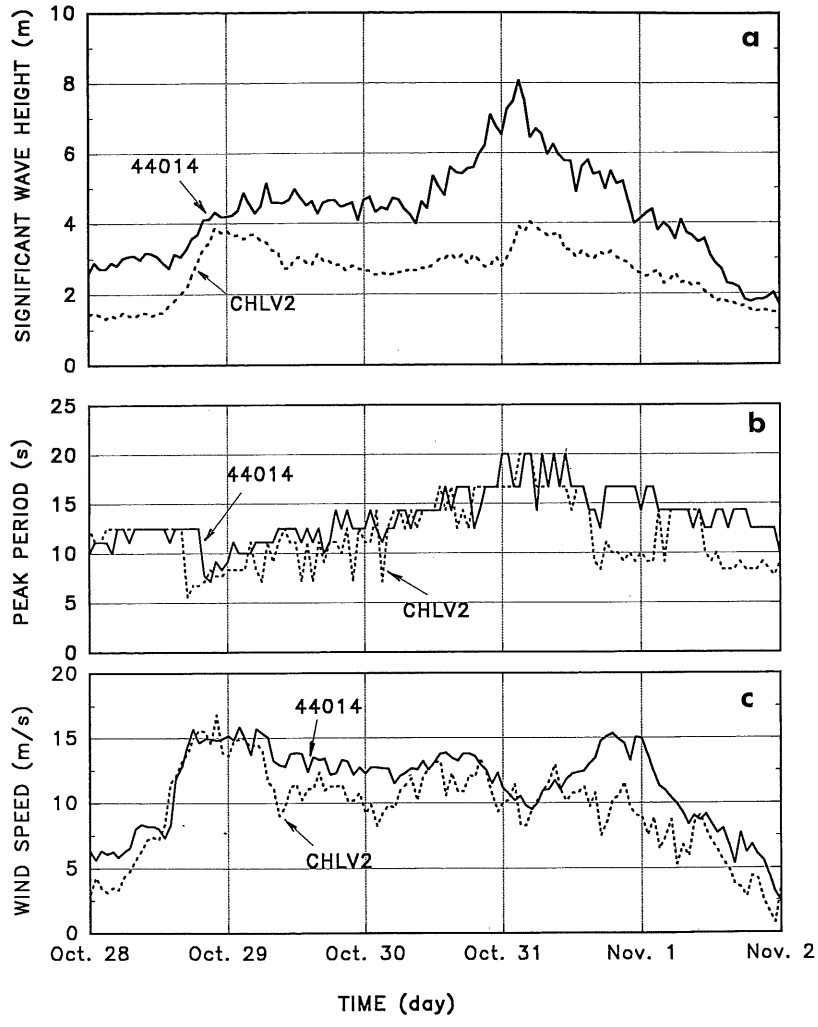

Figure 3. The evolution of significant wave height, peak wave period, and wind speed from October 29, 0 hr to November 1, 23 hr, 1991, GMT at station 44014 and CHLV2.

spectrum is relatively narrow banded. The wave energy is high and concentrated from 0.04 to 0.10 Hz (*i.e.*, from 25 to 10 sec) with a peak wave frequency of 0.06 Hz (period = 16.7 sec). The average wave spectrum at station CHLV2, however, is relatively broad banded. The range of wave energy variation at station CHLV2 is not significant (see the vertical bars in Figure 4). The significant wave height is 3.9 m.

Figure 5 shows the comparison of wave spectra at two other times: Oct. 30, 03:00 and Oct. 31, 10:00. The selected three pairs of spectra (Figures 4 and 5) represent different levels of wave energy recorded at station 44014. Before the storm peak, see Figure 5a, wave energy at station 44014 is relatively small and concentrated between 0.06 and 0.13 Hz. At the nearshore station, it is almost uniformly distributed between 0.06 and 0.14 Hz with a weak peak at 0.07 Hz. After the storm peak (see Figure 5b), the wave energy at station 44014 is medium and mainly between 0.05 and 0.10 Hz. Notice that the ratio of wave energy at peak frequencies between station 44014 and CHLV2 is about 4 for the small wave height (see Figure 5a).

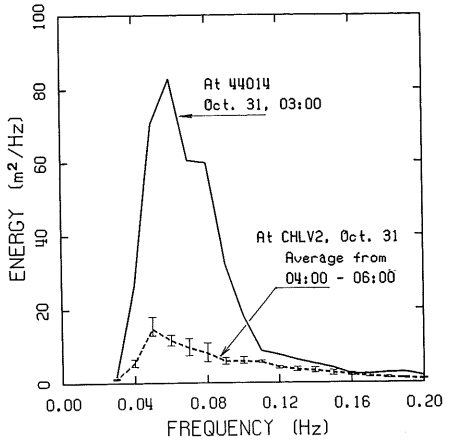

Figure 4. Comparison of measured wave spectra at storm peak (Oct. 31, 03:00, 1991 GMT) at station 44014 and station CHLV2. The bars indicate the range of wave energy spectrum for the three consecutive hours.

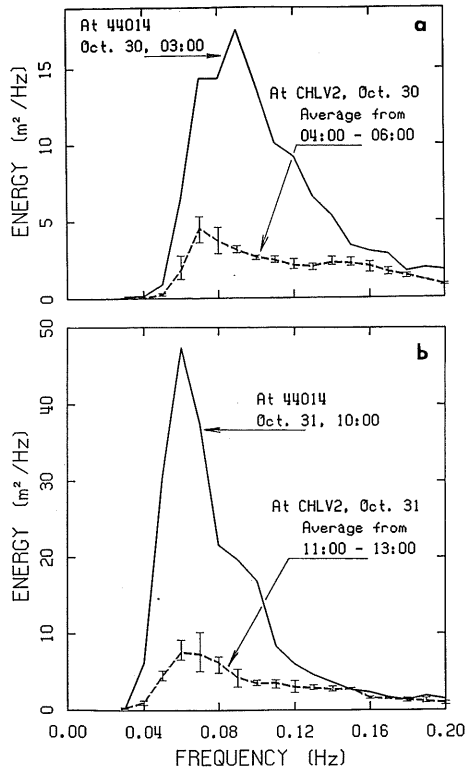

Figure 5. Comparison of the measured wave energy spectra at station 44014 and station CHLV2. (a) A small storm wave before peak; (b) A moderate storm wave after peak. The bars indicate the range of wave energy spectrum for the three consecutive hours.

For the moderate and large wave heights, the ratio is about 6.

Figure 6 shows the corresponding wave directions for the three selected times at station 44014 (angles are given as azimuths). We used the average of three consecutive wave direction records (in 3 hrs) for each frequency component to obtain a smoothed representative wave direction. The vertical bars indicate the range of wave direction during that three hours. For the storm peak, the directions for each frequency band are also displayed as the dashed line in Figure 6b. Notice that the variation of wave angles in the three consecutive hours is limited to $\pm 6°$ except for the lowest frequency wave component ($f = 0.04$ Hz) and some high-frequency components ($f \geq 0.12$ Hz). Thus the average wave directions given in Figure 6 well represent the wave directions for the spectra displayed in Figures 4 and 5. Notice that the wave angles for the high-frequency components are not too far apart (46 degrees to 57 degrees) for the three selected storm waves. The major difference lies in the low frequency components. At the peak of the storm, the long-period wave components come from 70 to 80 degrees. Before and after the storm peak, long-period waves come from 30 to 50 degrees. This phenomenon demonstrates the passing through of large swells (the destructive force of the Halloween storm) that were generated somewhere else. The low frequency waves ($f < 0.05$ Hz) shown in Figure 6a are mainly locally generated waves. The drastic change of wave direction for the low frequency wave component ($f = 0.04$ Hz) shown in Figure 6c further indicates the ending of these huge swells.

THE WAVE TRANSFORMATION MODEL

In this study, we used a modified version of the RCPWAVE model to examine wave refraction, diffraction, shoaling, and the effect of wave energy loss caused by bottom friction and percolation. This model solved the mild slope equation given by BERKHOFF (1972). Although it has been widely accepted, among others, by the coastal engineering community, it has two major limitations. (1) It can only simulate weak diffraction. In other words, the wave orthogonals must be roughly parallel (within $\pm 30°$) to the x coordinate of the compu-

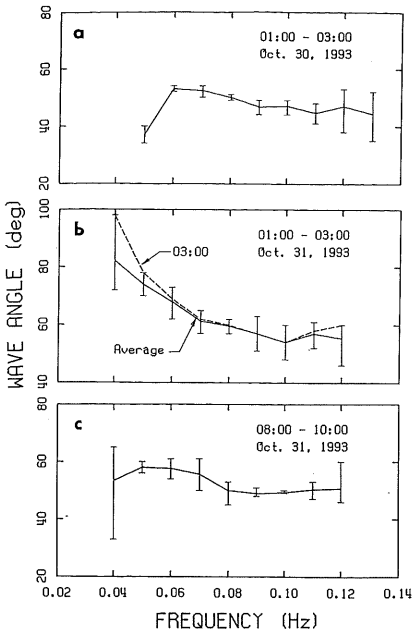

Figure 6. Measured wave directions for the three selected spectra at station 44014. The bars indicate the range of wave direction for the three consecutive hours.

tational grid. (2) It is a model for monochromatic waves. Simulation results using the significant wave height to represent the entire wave spectrum are poor (VINCENT and BRIGGS, 1988). This model, on the other hand, gives local wave angles by solving an extra equation, the irrotational condition. Thus we can calculate and plot wave rays using the computed local wave angles to demonstrate wave refraction and diffraction. The plot of wave rays is an added-on feature for displaying the results from the RCPWAVE model.

To compensate for the first limitation and save computing time, we used three small grids to calculate wave refraction and diffraction instead of two large grids, see Figure 2. The x axis of the grids were selected roughly parallel to the wave directions. Grid 1 was used to find the possible deepwater wave incident angles by comparing the measured and calculated wave angles at station 44014. Grids 2 and 3 were used to find the wave height for each wave component at station CHLV2. The selection of using Grid 2 or Grid 3 depends on the deepwater wave direction, with a goal of having the calculated local wave angles roughly parallel to the x-axis.

Table 1. *Representative wave heights, periods, and directions for the selected wave spectra at Station 44014.*

Seq. No.	Frequency Band (Hz)	Wave Energy $\Delta f_i S_i$ (M^2)	Wave Height H_i (m)	Period T_i (sec)	Observed Wave Angle (degree)	Estimated Deepwater A_i (degree)
1	0.05–0.06	0.0389	0.54	18.2	45	29
1	0.06–0.07	0.1041	0.91	15.4	53	41
1	0.07–0.08	0.1433	1.07	13.3	51	43
1	0.08–0.09	0.1593	1.13	11.7	48	43
1	0.09–0.10	0.1570	1.12	10.5	47	45
1	0.10–0.11	0.1199	0.98	9.5	46	46
1	0.11–0.12	0.0965	0.88	8.7	46	46
2	0.03–0.04	0.1417	1.06	28.6	86	84
2	0.04–0.05	0.4863	1.97	22.2	78	72
2	0.05–0.06	0.7671	2.48	18.2	71	60
2	0.06–0.07	0.7163	2.39	15.4	64	58
2	0.07–0.08	0.6014	2.19	13.3	60	57
2	0.08–0.09	0.4613	1.92	11.7	57	57
2	0.09–0.10	0.2530	1.42	10.5	57	57
2	0.10–0.11	0.1336	1.03	9.5	57	57
3	0.04–0.05	0.1865	1.22	22.2	56	32
3	0.05–0.06	0.3893	1.76	18.2	58	38
3	0.06–0.07	0.4241	1.84	15.4	56	46
3	0.07–0.08	0.2951	1.54	13.3	52	46
3	0.08–0.09	0.2060	1.28	11.7	49	46
3	0.09–0.10	0.1825	1.21	10.5	49	47
3	0.10–0.11	0.1260	1.00	9.5	49	49
3	0.11–0.12	0.0718	0.76	8.7	50	50

Seq. 1 represents a small storm wave occurred on Oct. 30, 03:00
Seq. 2 represents the peak storm wave occurred on Oct. 31, 03:00
Seq. 3 represents a moderate storm wave occurred on Oct. 31, 10:00

To relax the second limitation, we divided the spectra observed at station 44014 (see Figures 4 and 5) into seven or eight frequency bands. Each band has a bandwidth of 0.01 Hz. For each band, there is a representative wave period, T_i, band width, Δf_i, spectrum density, s_i, and root mean square wave height, H_i, which can be calculated as follows (DEAN and DALRYMPLE, 1992):

$$H_i = 2(2\Delta f_i s_i)^{1/2} \quad (1)$$

Table 1 gives these representative parameters. The selection of these frequency bands was arbitrary. Wave components with a frequency greater than 0.12 Hz are excluded because of the small wave energy in that domain. We then used the above deepwater wave information to calculate wave refraction, diffraction, shoaling, and bottom friction.

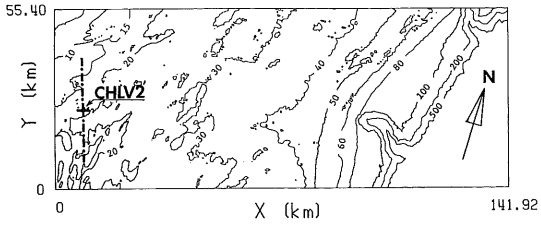

Figure 7. Water depth contours (in meter) for grid 2. Station CHLV2 is marked as "+" along with a transversal line (x = 8.795 km) for showing water depth and calculated wave heights later.

Because of the limitation of computer resources and the requirement of a large study area (141.92 km × 55.40 km, see Figure 7), we selected a large grid size, 160 m × 200 m. Thus, the wave diffraction may not be well simulated for the high frequency wave components.

PERCOLATION

Wave energy loss caused by percolation depends on the wave period, T, water depth, h, and sediment permeability, K (REID and KAJIURA, 1957; summarized in DEAN and DALRYMPLE, 1992). Equation 2 shows the wave amplitude decay coefficient k_i, defined as $a = a_0 \exp(-k_i x)$, as

$$k_i = \frac{2(\sigma K/\nu)k}{2kh + \sinh(2kh)} \quad (2)$$

where a_0 is the wave amplitude at $x = 0$, and a is the wave amplitude at x, $\sigma = 2\pi/T$, k is wave number, and ν is kinematic viscosity of water.

The permeability for sandy sediments can vary from 10^{-9} to 10^{-12} m^2. Because we do not know the permeability at the continental shelf off the Virginia coast, we chose a relatively large constant permeability, $K = 10^{-10}$ m^2 for the entire domain to examine the significance of this kind of wave energy loss. Assuming a 14 sec wave with water depth of 30 m (approximately the average depth between station CHLV2 and the continental shelf break) and $\nu = 10^{-6}$ m^2/sec, k_i would be about 5.8×10^{-7}. Over 87 km, wave amplitude would be decreased by about 5%. This small loss of wave energy can not explain the big difference of wave spectra between the two stations. Of course, if we chose $K = 10^{-9}$ m^2, the wave amplitude would be decreased by about 39%, and this kind of energy loss will be significant. At this time, however, without permeability data, we would like to stay with $K = 10^{-10}$ m^2, and examine the energy loss caused by bottom friction.

BOTTOM FRICTION

MAA and KIM (1992) adopted a procedure to determine the wave energy loss caused by bottom friction for a monochromatic wave. Their procedure will be applied here with some modifications. In their approach, the key parameter needed to be determined is the wave friction factor, f_w. To estimate f_w, we should consider the following three possible bed textures: (1) grain size of a smooth, non-movable bed, (2) ripple geometries, and (3) a smooth, movable bed without ripples. MADSEN *et al.* (1988) and MADSEN *et al.* (1990) suggested an approach for calculating the f_w caused by ripples for wave spectra. They found that the friction factor for random waves is smaller than that of regular waves because of the rounding of ripple crests by large waves in the wave spectrum. Their findings, however, are limited to the effects of ripple geometries. For the severe "Halloween" storm waves, all ripples were probably wiped out because of the large bed shear stress. Thus only the energy dissipation caused by carrying suspended sediments and skin friction is considered.

Wave friction factor is a function of bed roughness and the wave semi-excursion distance (NIELSEN, 1992). In this study, however, we selected using a constant f_w when the wave started "touching" the bottom ($d/L < 0.5$). This selection is based on certain conditions. (1) For this severe sea, ripples can not survive except in a small area close to the continental shelf break where the water depth is deep. Only the grain skin friction (usually small) and movable bed friction contribute to the wave energy loss. Thus the wave friction factor is reasonably constant and small (on the order of 0.01–0.05). An example of this condition has been demonstrated by MAA and KIM (1992). (2) A random sea has many wave components. The bed responses (the ripple geometry and sediment mobility), however, reflect the results of total wave energy instead of a single component. For a given sea, there exists only one bed form (from a statistical point of view), and different wave components may respond differently for the same bed form/mobility in terms of energy dissipation. These characteristics make estimating the f_w for each wave component difficult. For low amplitude, narrow banded waves, the approach given by MADSEN *et al.* (1988) may be applied.

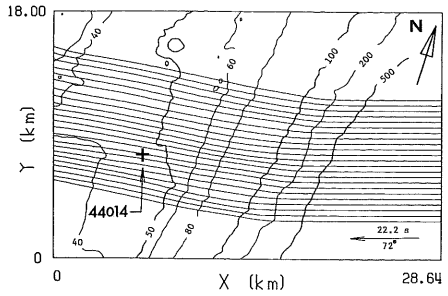

Figure 8. Wave trajectories show the possible incident and refracted wave direction for the 22.2 sec. Component wave at station 44014 on October 31, 03 hr, 1991, GMT.

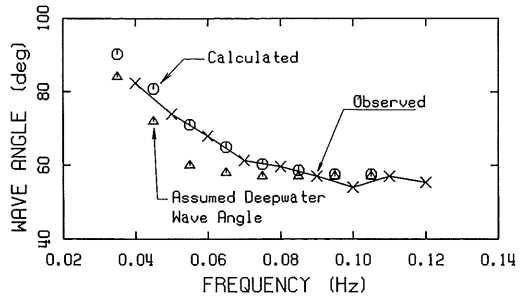

Figure 9. Comparison of the calculated and observed wave direction at station 44014 on October 31, 03 hr, 1991, GMT.

For a non-narrow banded spectrum, a practical formulation has not been established. Thus, using a constant f_w is the most feasible approach.

The energy loss, E_L, caused by the bottom friction in the wave propagation direction can be calculated as

$$E_L = \overline{\tau_b U_b}\Delta s = \frac{2}{3\pi}\rho f_w |U_b|^3 \Delta s \qquad (3)$$

where τ_b is the maximum wave bed shear stress, ρ is water density, Δs is the wave travel distance, and U_b is the maximum near-bed wave orbital velocity for a wave component. The wave attenuation coefficient, k_f, can be calculated as

$$k_f = \left(1 - \frac{E_L}{EC_g}\right)^{1/4} \qquad (4)$$

where $E = \rho g H^2/8$ is wave energy, C_g is wave group velocity, and H is local undamped wave height (wave height before considering the bottom friction). To estimate the attenuation of wave height caused by wave energy loss, we multiply H and k_f to obtain the attenuated wave height. It was used to find the undamped wave height at the next grid point and followed by the calculation of attenuated wave height at that point. This procedure was used for the entire wave propagation domain.

ESTIMATING DEEPWATER WAVE DIRECTION

A wave with frequency $\leq$ 0.10 Hz starts refracting at a water depth greater than 70 m. Thus, the measured wave directions at station 44014 for frequencies $\leq$ 0.10 Hz were already affected by the bottom topography. We need to estimate the deepwater wave directions to supply the boundary condition for the RCPWAVE model to calculate wave refraction and diffraction.

Although waves have traveled about 10 km from deepwater to station 44014, wave energy loss caused by the bottom friction is small because of the great water depth. When we use the observed wave direction information at this station to determine the deepwater wave direction A_i, we neglected the bottom friction.

Assuming a deepwater wave direction and using the wave information (T_i and H_i) given in Table 1, the bathymetry in Grid 1, and the RCPWAVE model, we calculated the wave transformation within Grid 1 for each frequency band. An example of this calculation, showing the wave rays for one of the frequency bands (T_i = 22.2 sec), is given in Figure 8. Comparing the calculated wave directions with the observed wave directions, we can estimate the deepwater incident wave direction off the continental shelf break. Figure 9 shows the comparison of calculated local wave angles and observed wave angles at station 44014 for each frequency band of the peak storm spectrum. The estimated deepwater wave angles for all three storm spectra are also listed in Table 1. For the storm peak, we found the deepwater wave direction to be 57 degrees for the high-frequency wave components (f_i > 0.06 Hz). For the low-frequency components, A_i increases as the frequency decreases (see Table 1). Notice that the observed wave direction for some low-frequency components (0.03 Hz or 0.04 Hz) are not accurate because the wave energy is low (see Figures 4 and 5), and thus these components are not plotted.

Table 2. *Calculated wave heights for each component at Station CHLV2 based on selected constant f_w.*

Seq. No.	Period T_i (sec)	Calculated Wave Height Using f_w = 0	0.01	0.02	0.03	Grid Used for Simulation
1	18.2	0.22	0.18*	0.17	0.16	3
1	15.4	0.43	0.39*	0.35	0.31	3
1	13.3	0.74	0.66	0.57*	0.50	3
1	11.7	1.65	1.29	1.04	0.88*	3
1	10.5	1.52	1.24	1.03	0.90*	3
1	9.5	0.79	0.67	0.59	0.50*	3
1	8.7	1.03	0.90	0.79	0.72*	3
2	28.6	1.22	0.58*	—	—	2
2	22.2	1.13	0.46*	0.40	0.33	2
2	18.2	1.09	0.79*	0.63	0.51	2
2	15.4	1.43	0.99*	0.75	0.60	2
2	13.3	2.00	1.29	0.94*	0.76	2
2	11.7	1.70	1.29	0.92	0.77*	2
2	10.5	1.30	0.59	0.83	0.74*	2
2	9.5	1.04	0.86	0.78	0.72*	2
3	22.2	0.15	0.08*	—	—	3
3	18.2	0.81	0.62*	0.52	—	3
3	15.4	0.88	0.70*	0.57	0.49	3
3	13.3	1.11	0.88	0.73*	0.63	3
3	11.7	1.84	1.35	1.04	0.83*	3
3	10.5	1.65	1.32	1.09	0.94*	3
3	9.5	1.22	1.02	0.87	0.78*	3
3	8.7	0.65	—	—	0.51*	3

*Selected to reconstruct the wave spectra at Station CHLV2

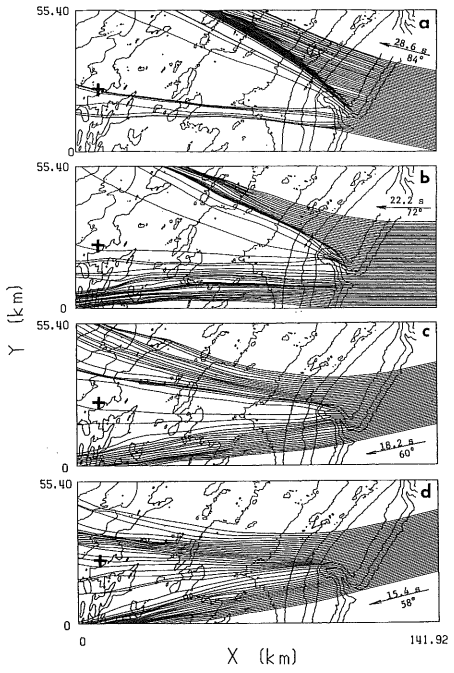

Figure 10. Wave rays for selected wave components on October 31, 03 hr, GMT. (a) For T = 28.6 sec; (b) For T = 22.2 sec; (c) For T = 18.2 sec; (d) For T = 15.4 sec. The plot of wave rays is an added-on feature for displaying RCPWAVE model results.

CALCULATED SPECTRA AT CHLV2 WITHOUT BOTTOM FRICTION

We then studied the wave transformation for each wave band using the T_i, H_i, A_i given in Table 1 and the bathymetry shown in Grid 2 or Grid 3. Our selections are given in Table 2. Bottom friction is not included at this time. Examples of calculated wave rays for selected frequency bands for the storm peak are given in Figure 10. This figure reveals that the Norfolk Canyon (at water depth from 100 to 500 m) causes low-frequency wave components to diverge. As the wave period decreases, the influence of the Norfolk Canyon decreases and is eventually negligible when the wave period is less than 14 sec. The Baltimore Canyon (see Figure 2) has a similar effect on the wave transformation, but the affected domain is mostly out of the study area.

Figure 11 shows computed wave height profiles for selected components of the peak storm spectrum along a transversal line that passes through station CHLV2 (see Figure 7). The water depth along this profile is displayed as the dotted line. The location of station CHLV2 is marked as well. We can see clearly that wave height varies along this line because of wave shoaling, diffraction, and refraction. The wave height at station CHLV2 for each component can be read from these profiles, and they are summarized in Table 2.

Using Equation 1, we calculated the wave energy for each frequency band given the calculated wave height of that band. The resultant spectrum for the storm peak is depicted in Figure 12. In general, the calculated wave energy is much larger than that recorded at station CHLV2. The only exceptions are for the 0.045 and 0.055 Hz component; the calculated wave energy is close to the observed at these bands because of the wave divergence, see Figure 10. For wave frequencies greater than 0.075 Hz, the calculated spectrum is almost equal to that at the offshore station. Notice that these results do not include the effect of possible wave growth over 87 km (from offshore to

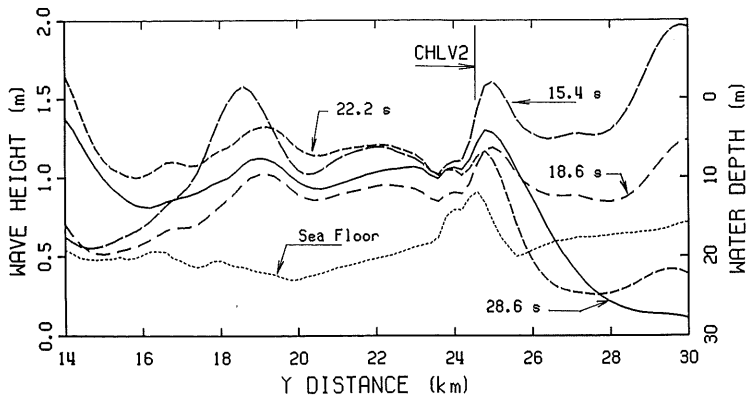

Figure 11. Calculated wave height profiles (without bottom friction) for selected wave components and bottom profile along the transversal line at X = 8.795 km.

station CHLV2). If considering any contribution from wave growth, the difference will be larger than those displayed in Figure 12.

CALCULATED SPECTRA AT CHLV2 WITH BOTTOM FRICTION

As we previously discussed, we use a constant f_w to study the effect of energy loss. We do not know, however, what the f_w is for each component. Thus, we found the best fit through trial and error ($0.01 < f_w < 0.05$). We calculated the wave heights at station CHLV2 for all the wave components with a given f_w and then constructed the wave spectrum (using Eqation 1) to compare with the measurements. The calculated wave heights are given in Table 2 for the three selected constant wave friction factors, $f_w = 0.01$, 0.02, and 0.03. The reconstructed wave spectra for all four wave friction factors of the peak storm wave are displayed in Figure 12. It reveals that using a small f_w to calculate wave energy loss at station CHLV2 for low-frequency wave components better matched the observations. For high-frequency wave components, we needed a relatively large f_w. Using the selected wave heights (marked by * in Table 2), we can reasonably reconstruct the wave spectra that are close to the observed spectra. Figure 13 shows the comparison of the three reconstructed and observed spectra at station CHLV2. In general, the calculated wave spectra show a shift of peak frequency. For low-frequency components, the calculated wave energy is smaller than that observed. For high-frequency components, however, the calculated wave energies are larger than the measured. We could try other small f_w, *e.g.*, 0.005, for the low-frequency components and large f_w for the high-frequency components to obtain better results. However, because of the following reasons, we stop at this point. (1) The point we want to make is that without considering energy loss caused by bottom friction (and others), the calculated wave spectra would be much larger than the observed. (2) The accuracy of measured deepwater wave incident angles is very important. Cur-

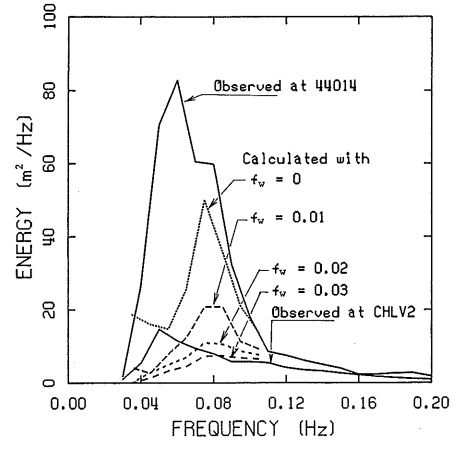

Figure 12. Comparison of measured and calculated wave spectra at station CHLV2 using different f_w for the peak storm wave.

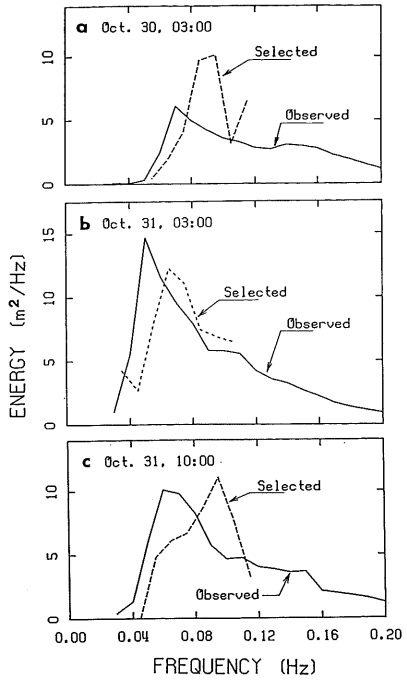

Figure 13. Comparison of measured and calculated wave spectra using selected f_w at station CHLV2. (a) For the small storm wave; (b) For the peak storm wave; (c) For the moderate storm wave.

rently the accuracy is limited to ±5 degrees, which may not be accurate enough for spending more effort to find the best-fit f_w. (3) The limited computing resources restricted our use of a fine grid size. (Ideally, the grid size should be less than ⅛ of the local wave length.) Thus, the wave diffraction process may not be well simulated. (4) Even if we can afford to use a small grid size, we are still limited by the accuracy of bathymetric data. We are already using the best data; however, for far offshore areas, the survey data are widely spaced and old. Thus, some basic uncertainties are involved. (5) Other possible processes that may affect the wave transformation (*e.g.*, wave-wave interactions, white capping, wave nonlinearity, etc.) should be examined first before launching another exercise. (6) At the offshore station, energy within a frequency band may comprise contributions from more than one direction. Even if there is just one major direction, there is some directional spreading around that major direction. Thus, wave energy from other directions should be considered to reconstruct a nearshore wave spectrum. This leads to another affordability problem as there are too many components to calculate. For this particular storm, we would like to demonstrate the importance of directional spreading by examining the peak storm wave as follows.

DIRECTIONAL SPREADING AND SENSITIVITY

For the storm peak at station 44014, the directional spreading for each component is given in Figure 14. Notice that part of the spreading shown in this figure is due to the directional resolution of the instrument and the analysis procedure. This figure shows that the wave directional spreading is not significant except for the low-frequency components (frequency ≤ 0.05 Hz). Wave energy at these frequencies came from a broad range of directions (from 50–110 degrees). This large spreading means that the incident wave angle (72 degrees) for the frequency band ($0.04 < f_i \leq 0.05$ Hz) may not be representative.

The large directional spreading of an incoming wave further complicates the spectral wave transformation because of additional wave energy from other directions. For this reason, the resultant wave profile given in Figure 11 would be smoother than that displayed. As a consequence, the reconstructed spectra would also be smoothed. We will show the sensitivity of this issue using the 0.045 Hz component as an example. If this wave component has an incident angle of 67 degrees (a 5 degree difference from that given in Figure 10b), the calculated wave height at station CHLV2 would be quite different. Figure 15 shows the comparison of calculated wave height profiles along the line shown in Figure 7. The difference in wave height at station CHLV2 is quite large, 0.5 m versus 1.13 m. This significant difference shows the importance of having accurate information on incident wave angle and the importance of the smoothing effect caused by wave directional spreading.

DISCUSSION

Field data for wave transformation, especially for extreme events, are scarce. The "Halloween" storm waves have been well observed along the east coast of the states. The data demonstrate the transformation of huge swells that cross the continental shelf, and provide excellent information for a case study.

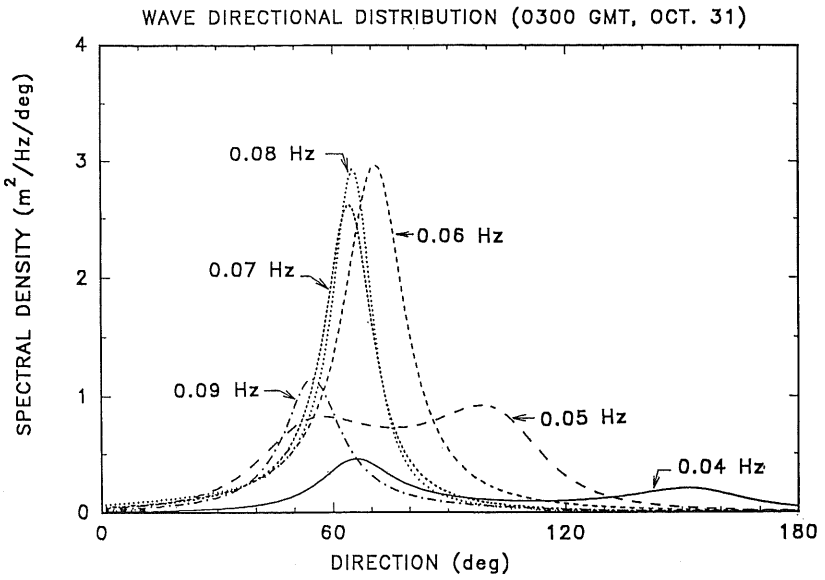

Figure 14. Directional spreading of each wave component at station 44014 on October 31, 03 hr, 1991, GMT.

It is impractical to account for the effect of bottom friction for random waves using a single representative f_w for the entire frequency range, especially when the wave energy is composed of a broad range of frequencies. In terms of energy loss, each wave component responds differently to a given bottom condition, which is controlled by the total wave energy. In this study, we used three small constant f_w's (0.01–0.03) for the storm waves because of the sea severity. When ripples do exist for small random waves, this assumption may not be valid because f_w may change significantly along a wave trajectory. In those cases, the approach given by MADSEN *et al.* (1988) may be applied.

Most of the wave components in this study are concentrated in one direction except the two low frequency bands (22.2 sec and 28.6 sec). Our selection of a single wave direction for these two frequency bands may be over-simplified. Considering the energy from other directions, the resulting wave spectrum would be smoother than using a single direction. More effort is needed to reconstruct a nearshore wave spectrum for cases where the directional spreading is large.

We have shown that the Norfolk Canyon, located at the continental shelf break, has a significant influence on wave refraction and diffraction for these low-frequency components of the "Halloween" storm waves.

The accuracy of deepwater incident wave direction is important. Should the incident wave direction change a little, say five degrees (at the margin of the instrument's accuracy), the wave at the nearshore station would be quite different. An example was given for the 22.2 sec wave component where a five degrees change in deepwater wave direction resulted in a 100% increase in the nearshore wave height for that component.

Because of the long-period waves, the influence of wind energy input on the calculation of wave height is limited. In our case, the distance between the two stations, 87 km, may not be long enough for a significant transfer of wave energy from high-frequency bands to low-frequency bands. Thus, in the calculation of wave height for the long-period wave components, the wind energy input is neglected. If this factor was considered, the calculated wave spectra would be even larger than that currently calculated. In other words, we would have to use large f_w's to reduce the calculated spectra in order to match the observations, especially for the high frequency component. On the other hand, since we neglected the possible

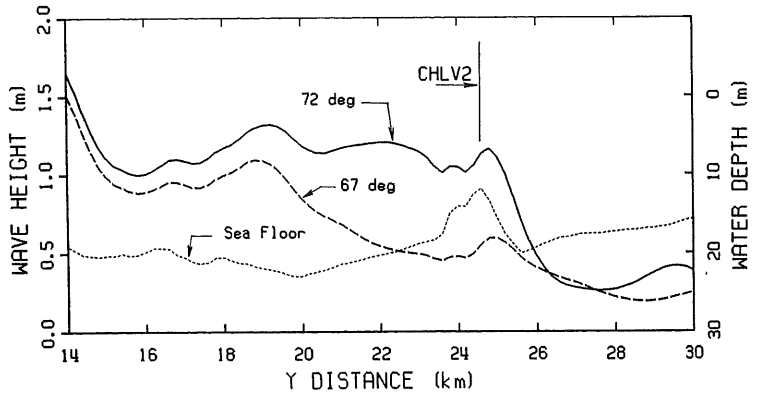

Figure 15. Calculated wave height profiles show the sensitivity of deepwater wave incident angle.

energy loss caused by percolation, white capping, and wave breaking, we may overestimate the f_w. The concluded weak relationship between f_w and wave frequency may indicate the necessity of considering other processes, such as those mentioned above, to better simulate this "Halloween" wave transformation.

As other studies have indicated, wave energy can be transferred among each wave component through wave-wave interactions. This process has not been addressed in this study, but it should be emphasized in the future.

Because of the great water depth (20–100 m) between the two stations and low frequency waves, the possible energy loss from wave breaking and white capping is not considered in this study. As we mentioned earlier, we are presenting a special event and trying to find possible reasons for the great difference in wave spectra between the two stations. Because we are not able to include all possible processes, we only discussed the effects of wave refraction, diffraction, shoaling, and bottom friction. We hope this paper will stimulate advanced studies to scrutinize other possible processes.

CONCLUSIONS

We presented a possible approach to study the spectral wave transformation for severe seas generated by the 1991 "Halloween" Northeaster at the continental shelf off the Virginia coast.

We found that the wave refraction, diffraction, and shoaling do have significant influences on wave transformation. For example, the low-frequency waves diverge due to the Norfolk Canyon located at the offshore break. However, when calculating the wave spectra for the nearshore station without considering energy loss caused by bottom friction, the high-frequency (from 0.08 and 0.12 Hz) wave energies are too large when compared to the observations.

Using a constant f_w for a wave component to calculate the wave energy loss is a practical approach for severe seas because all ripples were wiped out by the severe storm waves. Based on this limited study, we concluded that the wave friction factor, f_w, for long-period waves is smaller than that for short-period waves. The variation of f_w, however, is not significant.

Considering the effect of bottom friction, wave spectra at the nearshore station are much closer to the observations. Large errors (*e.g.*, 4–6 sec difference in peak period, and up to 50% error in energy at peak) still exist, and thus warrant additional studies.

This study indicates that accurate measurements of wave incident angles and the directional spreading at offshore stations are essential for a reliable prediction of wave transformations.

ACKNOWLEDGEMENTS

Sincere appreciation goes to Dr. R.G. Dean for his valuable comments. We also appreciate Mr. R. Lukens, Dr. A. Kuo, and Mr. J. Posenau for their support of the crucial computing resources. Mr. M.-H. Maa typed and proofread this manuscript. This paper is a contribution (No. 1919) of

the School of Marine Science, Virginia Institute of Marine Science, College of William and Mary.

LITERATURE CITED

ABREU, M.; LARRAZA, A., and THORNTON, E., 1992. Nonlinear transformation of directional wave spectra in shallow water. *Journal of Geophysical Research,* 97(C10), 15, 579–15, 590.

BERKHOFF, J.C.W., 1972. Computation of Combined Refraction-Diffraction. *Proceedings, 13th International Conference on Coastal Engineering* (ASCE), 1, 471–490.

BERKHOFF, J.C.W.; BOOY, N., and RADDER, A.C., 1982. Verification of numerical wave propagation models for simple harmonic linear water waves. *Coastal Engineering,* 6, 255–279.

BRIGGS, M.J.; GRACE, P., and JENSEN, R.E., 1989. *Directional Spectral Wave Transformation in the Nearshore Region, Report 1, Directional Spectral Performance Characteristics.* TR-CERC-89-14, CERC, Department of the Army, WES, USACE, Vicksburg, Mississippi 39180.

CHEN, Y.-H. and WANG, H., 1983. Numerical model for nonstationary shallow water wave spectrum transformations. *Journal of Geophysical Research,* 88(C14), 9851–9863.

CHIAIA, G.; DAMIANI, L., and PETEILLO, A., 1990. Wave Spectrum Transformations. *Proceedings, 22nd International Conference of Coastal Engineering* (ASCE), 1, 1102–1115.

DEAN, R.G. and DALRYMPLE, R.A., 1992. *Water Wave Mechanics for Engineers and Scientists.* 2nd printing, Singapore: World Scientific.

DOLAN, R. and DAVIS, R.E., 1992. Rating Northeasters. *Mariners Weather Log,* Winter 1992.

EBERSOLE, B.A.; CIALONE, M.A., and PRATER, M.D., 1986. *Regional Coastal Processes Numerical Modeling System, Report 1, A Linear Wave Propagation Model for Engineering Use.* TR-CERC-86-4, CERC, Department of the Army, WES, USACE, Vicksburg, Mississippi 39180.

KIRBY, J.T., 1986a. Higher-order approximations in the parabolic equation method for water waves. *Journal of Geophysical Research,* 91 (C1), 933–952.

KIRBY, J.T., 1986b. Rational approximations in the parabolic equation method for water waves. *Coastal Engineering,* 10, 355–378.

KIRBY, J.T., 1988. Parabolic waves computations in nonorthogonal coordinate systems. *Journal of Waterway, Port, Coastal, and Ocean Engineering* (ASCE), 114(6), 673–685.

IZUMIYA, T. and HORIKAWA, K., 1987. On the transformation of directional random waves under combined refraction and diffraction. *Coastal Engineering in Japan,* 30(1), 49–65.

LIU, P.L.-F. and TSAY, T.-K., 1985. Numerical prediction of wave transformation. *Journal of Waterway, Port, Coastal, and Ocean Engineering* (ASCE), 111(5), 843–855.

LIU, P.L.-F.; BOISSEVAIN, P.L.; EBERSOLE, B.A., and KRAUS, N.C., 1986. *Annotated Bibliography on Combined Wave Refraction and Diffraction, Miss. Paper CERC-86-10,* Coastal Engineering Research Center, Department of the Army, Waterways Experiment Station, Corps of Engineers, Vicksburg, Mississippi 39180.

LONGUET-HIGGINS, M.S.; CARTWRIGHT, D.E., and SMITH, N.D., 1963. Observations of the directional spectrum of sea waves using the motions of a floating buoy. *Ocean Wave Spectra,* New York: Prentice-Hall, pp. 111–136.

MAA, J.P.-Y. and KIM, C.-S., 1992. The effect of bottom friction on breaking waves using RCPWAVE model. *Journal of Waterway, Port, Coastal and Ocean Engineering* (ASCE), 118(4), 387–400.

MADSEN, O.S.; POON, Y.K., and GRABER, H.C., 1988. Spectral wave attenuation by bottom friction: Theory. *Proceedings, 21st International Conference of Coastal Engineering* (ASCE), 1, 492–504.

MADSEN, O.S.; MATHISEN, P.P., and ROSENGAUS, M.M., 1990. Movable bed friction factors for spectrum waves. *Proceedings, 22nd International Conference of Coastal Engineering* (ASCE), 1, 420–429.

MEINDL, E.A. and HAMILTON, G.D., 1992. Programs of the National Data Buoy Center. *Bulletin of the American Meteorological Society,* 73(7), 985–993.

NIELSEN, P., 1992. *Coastal Bottom Boundary Layers and Sediment Transport.* Singapore: World Scientific, 324p.

PANCHANG, V.G.; CUSHMAN-ROISIN, B., and PEARCE, B.R., 1988. Combined refraction-diffraction of short waves in large coastal regions. *Coastal Engineering,* 12(2), 133–156.

PUSCH, R.J. and AVILA, L.A., 1992. Atlantic hurricane season of 1991. *Monthly Weather Review* 120(11), 2671–2688.

REID, R.O. and KAJIURA, K., 1957. On the damping of gravity waves over a permeable sedbed. *Transactions, American Geophysical Union,* 38.

SUH, K.D. and DALRYMPLE, R.A., 1993. Application of angular spectrum model to simulation of irregular wave propagation. *Journal of Waterway, Port, Coastal and Ocean Engineering* (ASCE), 119(5), 505–520.

STEELE, K.E.; WANG, D.W.-C.; TENG, C.C., and LANG, N., 1990. Direction Wave Measurement with NDBC 3-meter Discus Buoys. *NDBC Report No. 1804-01.05.*

VINCENT, C.L. and BRIGGS, M.J., 1988. Refraction-diffraction of irregular waves over a mound. *Journal of Waterway, Port, Coastal and Ocean Engineering* (ASCE), 115(2), 269–284.

WANG, D.W.-C. and METTLACH, T., 1992. The Halloween Storm: Data observations from NDBC Stations. *Proceedings, 3rd International Workshop on Wave Hindcasting and Forecasting,* Environment Canada Atmospheric Environment Service, Downsview, Ontario, Canada, M3H 5T4, pp. 383–400.